coatings

MDPI

Article

Effect of Bath Composition on Titanium Anodization Using the Constant-Current Approach: A Crystallographic and Morphological Study

Lapo Gabellini [1], Nicola Calisi [1,2], Stefano Mauro Martinuzzi [2,3], Rosa Taurino [1,2], Massimo Innocenti [2,3], Tiberio Bacci [1,2], Francesca Borgioli [1,2], Emanuele Galvanetto [1,2] and Stefano Caporali [1,2,*]

[1] Department of Industrial Engineering, DIEF, University of Florence, Via di s. Marta 3, 50134 Florence, Italy; lapo.gabellini@unifi.it (L.G.); nicola.calisi@unifi.it (N.C.); rosa.taurino@unifi.it (R.T.); tiberio.bacci@unifi.it (T.B.); francesca.borgioli@unifi.it (F.B.); emanuele.galvanetto@unifi.it (E.G.)
[2] Consorzio Interuniversitario Nazionale di Scienza e Tecnologia dei Materiali, INSTM, Via G. Giusti 9, 50121 Florence, Italy; stefano.martinuzzi@unifi.it (S.M.M.); m.innocenti@unifi.it (M.I.)
[3] Chemistry Department "Ugo Schiff", DICUS, University of Florence, Via della Lastruccia 3–13, 50019 Sesto Fiorentino, Italy
* Correspondence: stefano.caporali@unifi.it

Abstract: Porous TiO_2 thin films were prepared via electrochemical anodization of commercial-grade titanium foils in baths containing variable amounts of ethylene glycol. X-Ray diffraction, scanning electron microscopy, and UV/visible spectroscopy were employed to assess the effect of ethylene glycol on the nature of TiO_2 layers. Emphasis is given to the modification of pore size and anatase-to-rutile ratio since these characteristics strongly affect the catalytic performance of TiO_2. To simplify the scaling up of the process, a single-step anodization process was employed on a commercial grade 2 titanium foil in constant-current mode without the use of fluorides—conditions that are easily replicable on an industrial scale. We point out some interesting relationships among operating parameters, such as bath composition and current densities, and the characteristics of the anodization layers evidence that the pore size and anatase-to-rutile ratio can be strictly controlled. Increasing the amount of ethylene glycol stimulated the formation of a thinner and less porous TiO_2 layer, richer in rutile phase, and characterized by reduced-diameter pores. These results demonstrate the effectiveness and, to some extent, the tunability of the morphology and mineralogic composition of titanium anodization in fluoride-free and ethylene-glycol-bearing acidic solutions.

Keywords: anatase; rutile; anodization; titanium; ethylene glycol; nanoporous titania; XRD

Citation: Gabellini, L.; Calisi, N.; Martinuzzi, S.M.; Taurino, R.; Innocenti, M.; Bacci, T.; Borgioli, F.; Galvanetto, E.; Caporali, S. Effect of Bath Composition on Titanium Anodization Using the Constant-Current Approach: A Crystallographic and Morphological Study. *Coatings* **2023**, *13*, 1284. https://doi.org/10.3390/coatings13071284

Academic Editor: Frederic Sanchette

Received: 20 June 2023
Revised: 16 July 2023
Accepted: 19 July 2023
Published: 21 July 2023

1. Introduction

Titanium dioxide, despite recent concerns about its toxicity and suspected carcinogenicity [1], is an intensively researched and widely employed, low-cost material. It exists mainly in four different allotropic phases (amorphous, brookite, anatase, and rutile) which are characterized by different structural and physical properties. These phases can also form a large variety of architectures ranging from compact to porous layers, as well as nanotube or nanowire arrays [2–4]. Those architectures are the object of interest due to the possibility of them being used not only as hosting or templating substrates [5–7] but also as catalysts. Indeed, titanium oxide exhibits good photocatalytic properties toward the degradation of organic pollutants [8,9], an activity that can be significatively increased when the architecture of the catalyst is organized to maximize the exposed surface and the suitable crystalline form. According to these requisites, the candidate material should match the right arrangement at the atomic, nano, and micrometric scales. Generally speaking, among the various allotropes of titanium oxide [10,11], anatase is considered to possess the best photocatalytic efficiency with an activity exceeding that possessed by rutile and the amorphous phase [11].

There are several reported methods to obtain TiO_2 catalysts; however, among those, anodization from acidic solutions seems to be the simplest and least expensive [12–17]. This technique returns layers strongly bonded to the substrate, which, being made of titanium, is conductive, exhibits heat resistance, and possesses good chemical stability. Moreover, the obtained layer is usually porous [14]; moreover, it can be crystalline, and, as a function of to the environment and the anodizing parameters employed, traces of the electrolytes can be incorporated [11,14,18]. As with aluminum [19,20], titanium anodization can be performed under potential or current control. In this research paper, we adopt the current control approach, whereby we fix the current value, leading the voltage value to vary as a function of the electrical behavior of the system (mainly solution conductivity and insulating properties of the growing oxide). This requires a simpler experimental setup which can be more easily scaled up to an industrial level. Moreover, the choice of a well-stabilized power supply can reduce the fluctuations in the electrical parameters, leading the voltage to establish its value as a function of the path followed by the oxide layer growth [14]. This mechanism consists of the formation of an insulating material (titanium oxide, via a mechanism that is still debated in the detailed process) in equilibrium (in terms of conductivity and thickness) via anodic spark deposition (ASD). This latter phenomenon occurs with the onset of a small and well-distributed discharge on the anode's surface, leading to a rapid formation of titanium oxide and accounting for the growth of high porous and, generally, crystalline oxide layer [14]. It has been proven that the experimental condition of anodization may affect crystallinity, composition, and morphology [12–17,21–28] with a putative large tunability. Anodizing is usually performed in acidic environments [12,16,18,21], but several other solution compositions such as ionic liquids [29], nitrate ions with alcohols [30], phosphates [16,27,28,31], and bicarbonates [32] have been proposed and tested. Since ethylene glycol, in combination with fluoride [33], is widely employed for the fabrication of TiO_2 nanopores and nanotubes, we chose to study the effect of its addition on well-characterized anodizing solutions [14]. Regarding the non-ordinated porous TiO_2 layers, the effect of small amounts of EG (maximum 5% by volume) on the acidic bath was studied by Razzaboni and coworkers [34], who achieved nanocrystalline deposits exhibiting outstanding photocatalytic properties. In ordered nanoporous and nanotubular structures, the effect induced by water addition in EG solutions was also investigated [35], along with the effect of temperature and fluoride concentration [36–38]. Taking into account these studies, we focus on the effect induced by the variation of EG content in terms of morphology, mineralogic composition, and process efficiency. Employing a much wider EG content and, in the absence of fluoride ions, we aim to understand how the use of such a compound alone may constitute a practical and effective way to tailor the morphology and the anatase/rutile ratio of anodized TiO_2 layers, constituting a cheap and robust way for the realization of catalytic surfaces.

2. Materials and Methods

Commercial pure titanium (grade 2 according to ASTM B265 classification) specimens (30 mm × 30 mm × 1.5 mm) were cut from a hot-rolled foil and used as substrate. All samples were oriented parallel to the rolling direction to avoid preferential orientation. Before anodization treatment, the samples were mechanically polished using SiC abrasive papers down to P1200 grit, cleaned with detergent, water, and acetone, and then air-dried. Several layers of Kapton tape masked the sample's upper half, leaving a surface of 10 cm^2 ready to be treated. The anodizing process was carried out using the constant-current mode, with a two-electrode setup, wherein the anode constituted the titanium sample. It was inserted in a polypropylene cell surrounded by a grid of AISI 316l stainless steel constituting the cathode. The power supply was a computer-controlled generator TDKlambda ser 3.3 kW-2U (TDKlambda, Tokyo, Japan). Four different current densities (20, 40, 80, and 100 $mA \cdot cm^{-2}$) were tested to anodize 10 cm^2 of titanium, an area delimited on the titanium surface by means of a Kapton tape, selecting two opposite faces of the specimen. Regarding the bath composition, five different electrolytic aqueous solutions were tested: all of which

contained 0.5 M sulfuric acid (Sigma-Aldrich, Darmstadt, Germany) and different amounts of ethylene glycol (EG) (0%, 20%, 40%, 60%, and 80% v/v quantities). To characterize the nature of the oxides formed, XRD analysis (D8 Advance, Bruker, Santa Barbara, CA, USA) was carried out using Bragg Brentano geometry, collecting the diffraction patterns in the diagnostic range of anatase and rutile (24°–29°), with a 2.5 s step of 0.02°. To control the substrate, we collected XRD diffractograms from 20° to 65°, with a 0.05° step of 1 s. All data were collected using a slit of 0.2 mm. Diffractograms were fitted using MAUD software (version 2.94) [39] and CIF files of anatase and rutile available on COD [40,41] to calculate the percentage of the forming crystallographic phases. After graphitization, the morphology of the anodized layers was investigated using an SU3800 scanning electron microscope (Hitachi High-Tech, Tokyo, Japan), equipped with an Ultim Max 40 silicon drift energy-dispersive analyzer (Oxford Instruments, Wiesbaden, Germany). Bandgap measurements were performed using a UV/Vis spectrophotometer Cary 300 (Agilent, Santa Clara, CA, USA) in reflectance mode counting 0.1 s for every 1 nm step, followed by data processing using the method suggested by Makula and coworkers [42].

3. Results

3.1. Substrate Characterization

Prior to the anodization step, the substrate was prepared following the method described in Section 2 and then characterized using XRD to assess the absence of a significant number of crystalline oxides. Figure 1 reports the extended XRD diffractogram of titanium substrate, showing the peaks attributable to the alpha phase alone. The relative intensity of the diffraction peaks slightly differed from the standard PDF 44-1294 pattern, indicating an iso-orientation, probably arising from the manufacturing (hot rolling) step. The region between 24° and 29°, characteristic for the anatase (101) and rutile (110) diffraction peaks, and classically used to determine their relative intensities [14], did not display noticeable diffraction peaks, indicating the absence of detectable amounts of these oxides in the substrates.

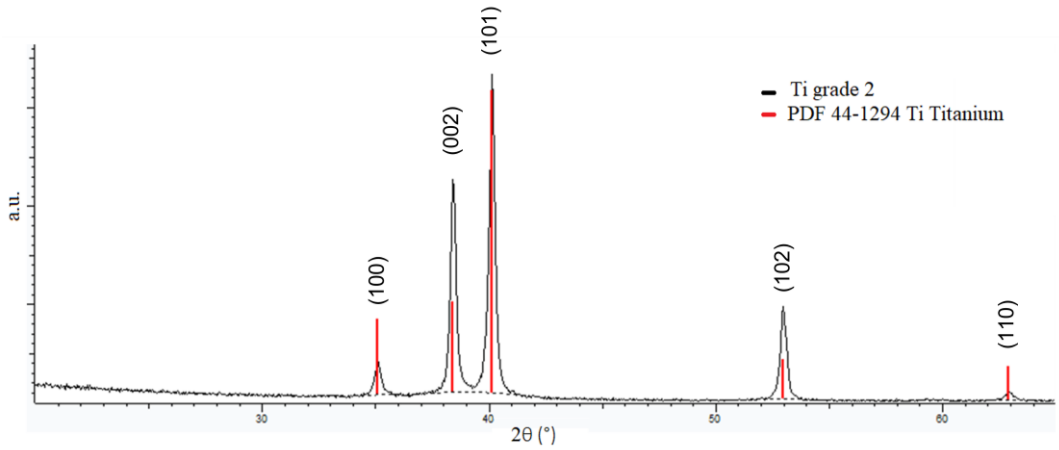

Figure 1. XRD data showing the absence of anatase or rutile peaks in the diagnostic region of 24°–29°. The extended region between 20° and 65° shows a small iso-orientation of the grade 2 titanium foil, imputable to the manufacturing. The plot was realized using diffracEva software (Bruker, Santa Barbara, CA, USA) (version 7); red bars are relative to JCPDS card number 44-1294 (alpha titanium).

3.2. Anodizing Treatment Conditions

The anodization process was carried out aiming to determine the effect of three different experimental parameters: (a) ethylene glycol amount, (b) current density, and (c) process duration.

Thus, following the work of Diamanti and coworkers [14], we chose to operate in acidic bath containing 0.5 mol·L^{-1} of H_2SO_4 and variable amounts of water and ethylene glycol (EG). To assess the effect of its addition to the aqueous solution, five anodizing baths

were prepared. These are listed in Table 1, named A to E. All of them were employed to produce anodized samples at a current density of 80 mA·cm^{-2} for 120 s.

Table 1. Composition of the anodization baths as ethylene glycol (EG) and water.

Solution	EG%	H_2O%
A [1]	0	100
B [1]	20	80
C [1]	40	60
D [1]	60	40
E [1]	80	20

[1] H_2SO_4 (0.5 M).

To determine the effect of current density, we operated at 20, 40, 80, and 100 mA·cm^{-2} using the bath composition identified as B (see Table 1), limiting the process duration to 120 s.

Finally, the effect of treatment duration was evaluated, for bath B, operating at 20 mA·cm^{-2} current density and extending the anodizing time to 300 and 600 s, respectively.

The potential–time transients obtained, while varying the current densities and the bath composition, are displayed in Figure 2A,B, respectively. They closely resemble the classical ones obtained for titanium in acidic aqueous solution.

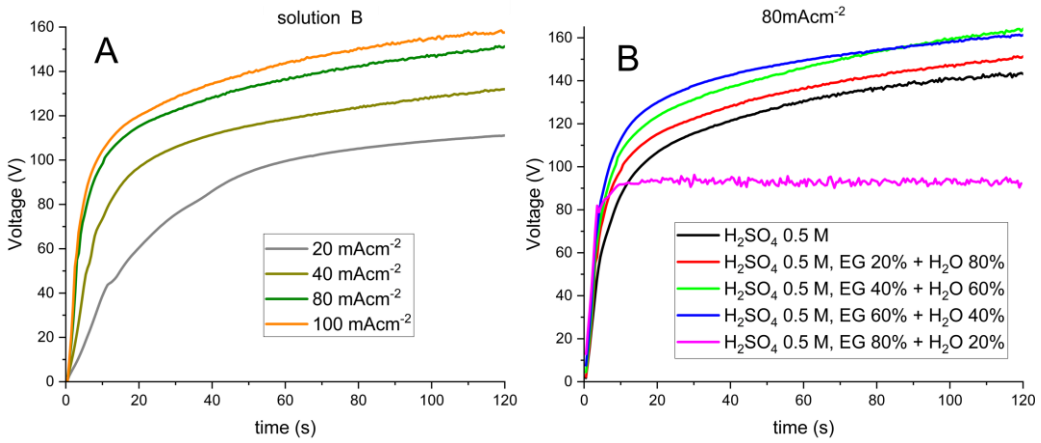

Figure 2. Potential vs. time transients obtained during titanium anodization in acidic aqueous solution. (**A**) Same composition but different current densities. (**B**) Same current density (80 mA·cm^{-2}) but different bath compositions.

The potential vs. time transients are characterized by a steep voltage increase, followed by a pseudo-linear behavior, ending in a nearly constant value at about 100–120 s. As expected, a higher current density led to higher final potential results (Figure 2A).

On the other hand, increasing the amount of EG returned steeper transients and higher final potentials, except for a very high content (solution E, 80% EG), which, after reaching 93 V, started a regime of sharp potential fluctuations that were probably due to local voltage-induced breakage of the growing oxide (Figure 2B).

3.3. Mineralogical Composition

Diffractograms collected in the diagnostic region of anatase (101) and rutile (110) are presented in Figure 3. It is worth noting that the three operative variables investigated returned three different effects. The increase in EG content in the bath composition resulted in a diminishing of both anatase and rutile. However, anatase formation was more inhibited than rutile formation (Figure 3C). Current densities affected the relative abundance of rutile and anatase; lower current density returned nearly pure anatase, whereas increasing the current density stimulated the production of rutile that almost reached 20% at 100 mA·cm^{-2}

(Figure 3A). Lastly, anodizing time did not affect the mineralogical composition of the film. The coatings produced with treatment lasting for 600 s were still composed exclusively of anatase (Figure 3B). Tables 2 and 3 summarize these data in terms of mineralogical composition and potential reached during the anodization.

3.4. Morphological Investigation

The anodized samples were characterized by a variable degree of porosity. The layer produced from solution A (0% EG, Figure 4A) showed a highly porous surface, while the sample produced using solution E (80% EG, Figure 4B) was characterized by the absence of pores and showed large portions of the surface interrupted by the presence of large depressions and cracks.

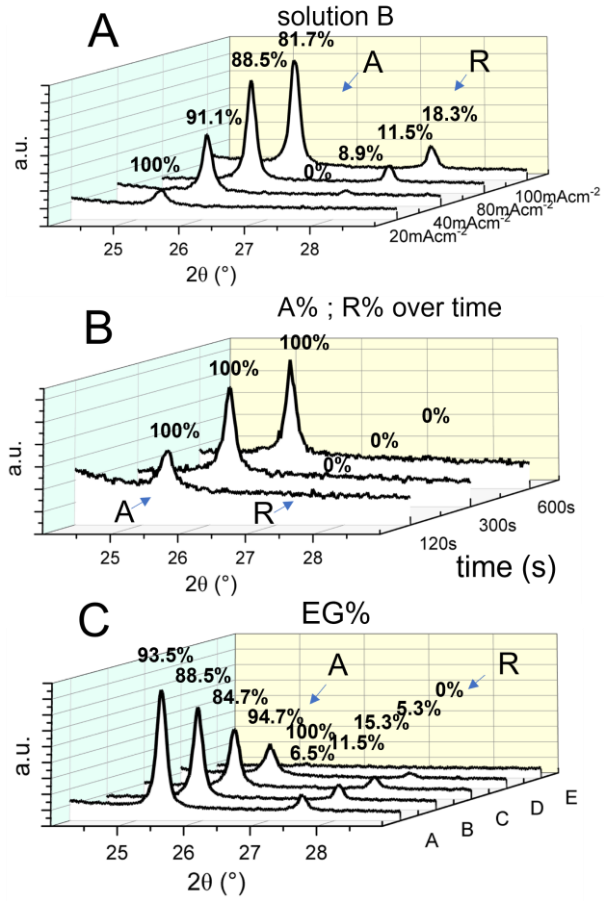

Figure 3. Representation of the peaks attributable to anatase (A) and rutile (R) in the XRD diagnostic region. The relative percentage of the two crystallographic phases is also reported. (**A**) Samples produced at different current density. (**B**) Effect induced by different treatment times at 20mA·cm^{-2}. (**C**) Effect induced by the anodizing bath composition (A to E).

Table 2. Anatase /rutile (A/R) abundance and final potential as a function of bath composition.

Solution	Current (mA·cm^{-2})	% (A/ R)	End Potential (V)
A	80	(93.5/ 6.5)	142
B	80	(88.5/ 11.5)	151
C	80	(84.7/ 15.3)	162
D	80	(94.7/ 5.3)	160
E	80	(100/ 0)	93

Table 3. Anatase/rutile (A/R) abundance and final potential as function of current densities and anodizing time.

Solution (Process Time)	Current (mA·cm^{-2})	% (A/ R)	End Potential (V)
B (120 s)	20	(100/ 0)	109
	40	(91.1/ 8.9)	130
	80	(88.5/ 11.5)	151
	100	(81.7/ 15.3)	157
B (300 s)	20	(100/ 0)	123
B (600 s)	20	(100/ 0)	125

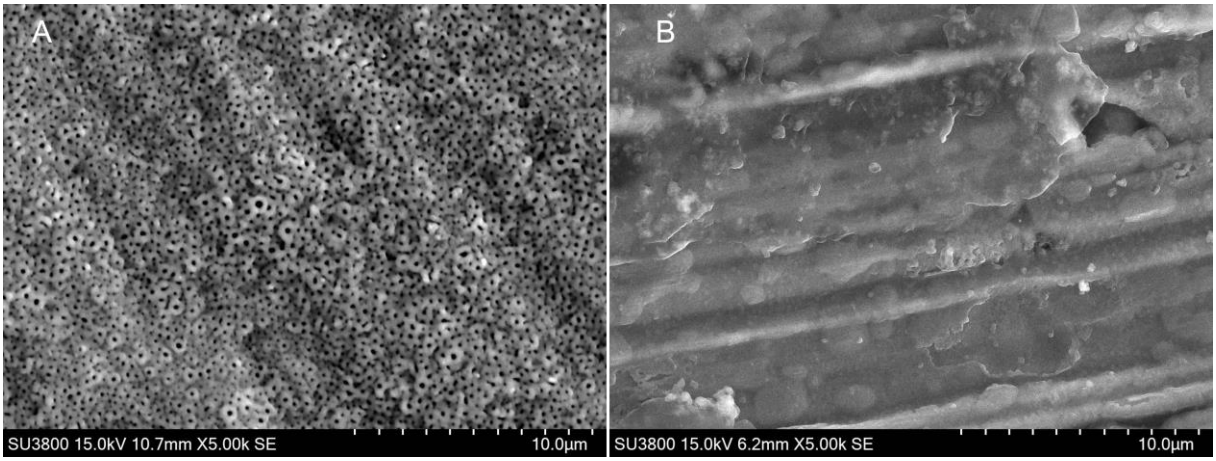

Figure 4. SEM images of TiO_2 layers produced at 80 mA·cm^{-2} in different baths: (**A**) bath type A; (**B**) bath type E.

As depicted in Figure 5, the increase in EG content (from 0% to 60% EG) returned coatings characterized by the presence of fewer and smaller pores. The increase in current density led to the formation of a more porous film (higher number of pores), as depicted in Figure 6. The same image also reveals the effect induced by an increase in the treatment time (Figure 6A–F), which also returned a more porous layer.

3.5. Bandgap and Chemical Composition

The bandgap measurement, carried out as described in Section 2, did not return unexpected results: 3.5 eV with negligible variation among the samples. Regarding the chemical composition, EDS analyses evidenced, along with titanium and oxygen, the presence of sulfur (values around 0.5%–1%, see Table 4). The amount of sulfur increased at higher current densities, while the duration of the anodization did not affect its content. Conversely, the addition of EG resulted in slight changes in the sulfur content, which assumed the highest value for EG content of 40% v/v. Incorporation of sulfate ions from the anodization bath is the more suitable explanation for such an occurrence.

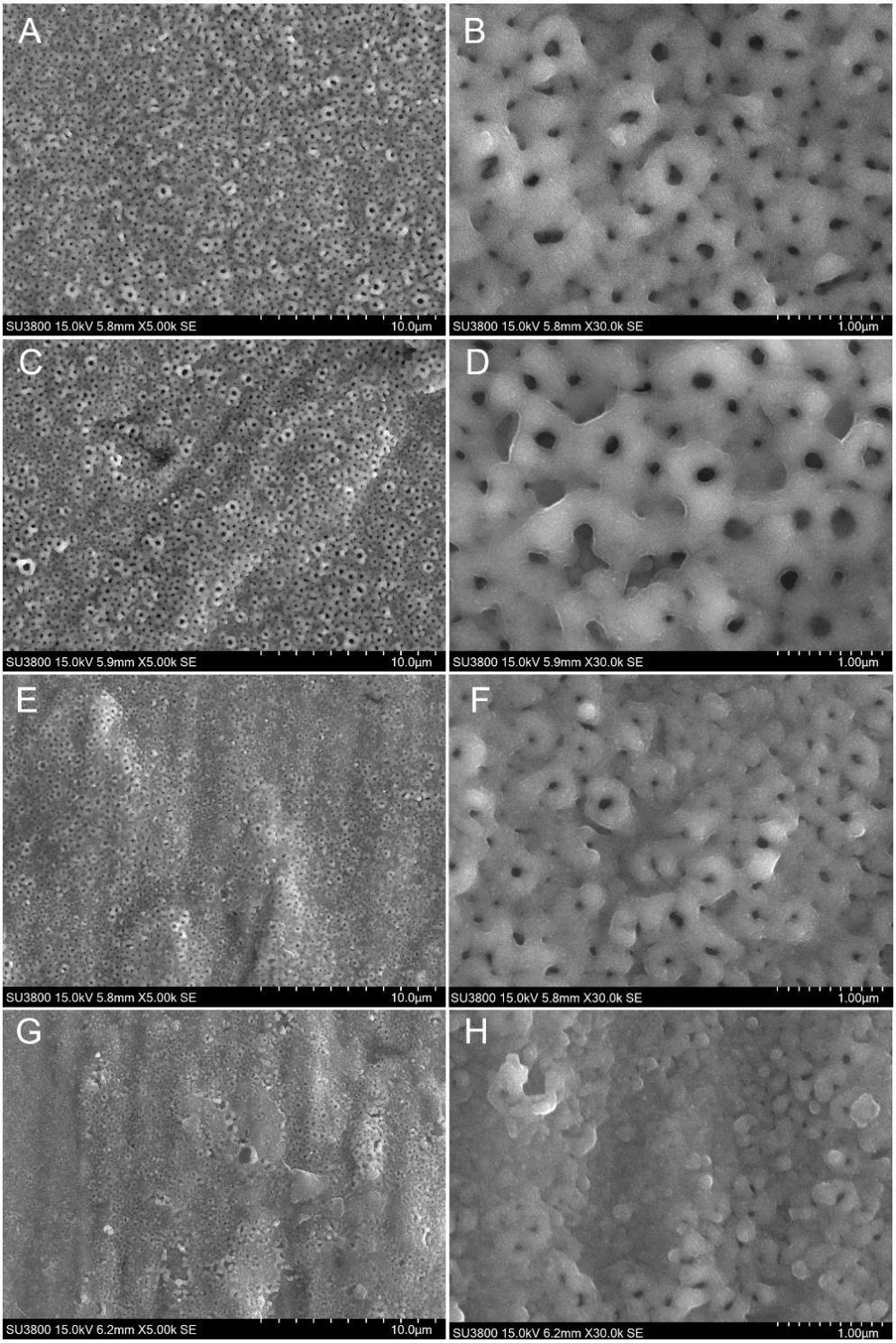

Figure 5. SEM images of TiO_2 samples obtained at 80 mA·cm^{-2} at different magnification (left 5000×; right 30,000×): (**A**,**B**) samples produced in solution A; (**C**,**D**) samples produced in solution B; (**E**,**F**) samples produced in solution C; (**G**,**H**) samples produced in solution D.

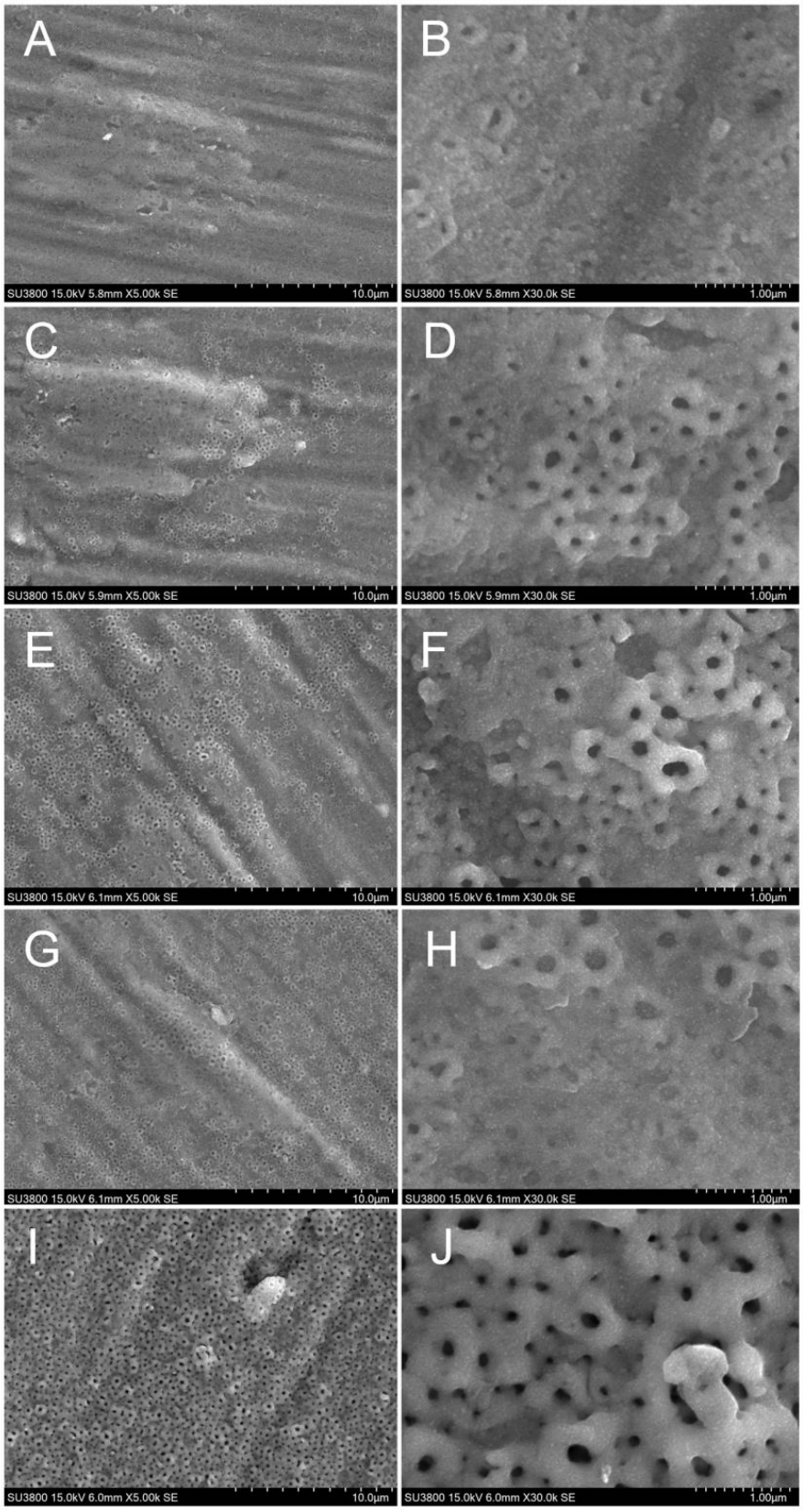

Figure 6. Morphologies of TiO_2 films realized in solution B (left 5000×; right 30,000×). (**A**–**F**) Samples produced at 20 mA·cm^{-2} for three different durations: (**A**,**B**) = 120 s; (**C**,**D**) = 300 s; (**E**,**F**) = 600 s. (**G**,**H**) Samples produced at 40 mA·cm^{-2} for 120 s. (**I**,**J**) Samples produced at 100 mA·cm^{-2} for 120 s.

Table 4. Sulfur content and final potential as function of anodization parameters.

Bath Type	Current (mA·cm^{-2})	% S (Weight)	End Potential (V)
B	20	0.39	109
	40	0.36	130
	80	0.61	151
	100	0.63	157
B (300 s)	20	0.44	123
B (600 s)	20	0.36	125
A	80	0.50	142
C	80	0.99	162
D	80	0.82	160
E	80	0.36	93

4. Discussion

The data presented in Tables 2 and 3 allow us to identify some interesting correlations between the anodizing parameters and the nature of the TiO_2 film. The addition of EG up to 60% v/v reduced the intensity of the diffraction peaks, especially regarding the anatase phase. When EG became even more abundant (80% v/v, bath type E), the peaks related to both crystalline phases almost disappeared. Since the diffractogram baseline did not increase and the coating macroscopically showed interferential coloration, the formation of a thinner TiO_2 layer can be concluded. Since the charge flown during the treatment was the same, it can also be concluded that the addition of EG reduced the efficiency of the anodization process. Small current densities stimulated the selective formation of anatase, with anodization layers that presented few pores, whose number increased over time without changing the mineralogical composition. Even after 600 s of anodizing, the peaks reported in Figure 3B showed the formation of a layer composed of almost pure anatase. Higher current densities returned higher end-voltages and, as already reported by other authors [14], a larger amount of rutile and an increased number of pores. By comparing Figures 4 and 5, the role played by EG can be revealed; larger amounts of EG led to the formation of smaller pores. A similar finding was observed by Rudnev and coworkers [43], which was explained on the basis of the work by Guo and An [44]. This latter study reported that the addition of a surfactant to the anodizing solution for the plasma electrolytic oxidation (PEO) process reduces the porosity of the oxide layer. This is a consequence of the reduced surface tension between the solid/liquid and liquid/gas interfaces [44], which leads to the formation of smaller oxygen bubbles. These bubbles are proposed to play a molding effect [45] on the growing oxide layer, resulting in the formation of smaller pores. A similar trend was observed by Berg and coworkers [46], who reported that the addition of water to a fluoride-bearing EG solution led to the formation of larger TiO_2 nanotubes [46]. On the other hand, the efficiency reduction observed for high EG content is reasonably attributable to the electro-oxidation of EG which is known to be catalyzed by TiO_2 [35]. Lastly, the cracked anodization layer observed in solution E may have been the result of the formation of a thinner and pore-free TiO_2 layer, which presented a lower breakdown voltage unable to reach the onset of ASD and, therefore, achieve the formation of pores.

The steep slope in the initial part of the time vs. potential transient was directly related to both current density and EG amount. While the trend observed by varying the current density can reasonably be explained by a higher formation of oxide over time, the effect induced by the variation of the EG% can be explained by considering the different conductivity of the solution. The mineralogical composition of the oxide layer is similar to that observed by other authors who reported the formation of rutile at potential values higher than 110–130 V [11], whereby the EG-containing solutions are situated in the upper limit of this range.

5. Conclusions

This work evaluated the mineralogical and morphological effect induced by different anodizing conditions, particularly the EG content, on the formation of titanium oxide layers. We found that EG reduced the thickness of the oxide layer and, by impairing the formation of anatase, affected the anatase-to-rutile ratio. This could be due to the higher insulating properties of the growing layer, which generates higher potential values favoring the formation of rutile. Lastly, we also confirmed that the layers produced using this approach are porous, with a porosity that becomes more evident using higher current densities and a longer treatment time. Conversely, porosity becomes less evident using a higher amount of EG%. Therefore, through appropriate tuning of these operating parameters, an appropriate morphology and anatase-to-rutile ratio can be achieved via a one-step process.

Author Contributions: Conceptualization, L.G. and S.C.; investigation, L.G., S.M.M. and N.C.; data curation, L.G., F.B. and E.G.; writing—original draft preparation, L.G.; writing—review and editing, S.C., S.M.M., N.C. and R.T.; visualization, T.B. and M.I.; funding acquisition, S.C. All authors have read and agreed to the published version of the manuscript.

Funding: This research received no external funding.

Institutional Review Board Statement: Not applicable.

Informed Consent Statement: Not applicable.

Data Availability Statement: The experimental data are reported in the article.

Acknowledgments: The authors acknowledge the technical support and facilities from the Match-Lab (Material characterization Laboratory) and Crist (Centro Servizi Cristallografia Strutturale) of University of Florence.

Conflicts of Interest: The authors declare no conflict of interest.

References

1. Kim, K.T.; Eo, M.Y.; Nguyen TT, H.; Kim, S.M. General review of titanium toxicity. *Int. J. Implant Dent.* **2019**, *5*, 10. [CrossRef] [PubMed]
2. Julkapli, N.M.; Bagheri, S.; Bee Abd, S.H. Recent Advances in Heterogeneous Photocatalytic Decolorization of Synthetic Dyes. *Sci. World J.* **2014**, *2014*, 692307. [CrossRef] [PubMed]
3. Vydianathan, K.; Nuesca, G.; Peterson, G.; Eisenbraun, E.; Kaloyeros, A.; Sullivan, J.; Han, B. Metalorganic chemical vapor deposition of titanium oxide for microelectronics applications. *J. Mater. Res.* **2001**, *16*, 1838–1849. [CrossRef]
4. De Nardo, L.; Raffaini, G.; Ebramzadeh, E.; Ganazzoli, F. Titanium oxide modeling and design for innovative biomedical surfaces: A concise review. *Int. J. Artif. Organs* **2012**, *35*, 629–641. [CrossRef]
5. Eswaramoorthi, I.; Lian-Pin, H. Anodic titanium oxide: A new template for the synthesis of larger diameter multi-walled carbon nanotubes. *Diam. Relat. Mater.* **2007**, *16*, 1571–1578. [CrossRef]
6. Eswaramoorthi, I.; Lian-Pin, H. Synthesis and characterisation of larger diameter multi-walled carbon nanotubes over anodic titanium oxide template. *Carbon* **2006**, *44*, 2341–2344. [CrossRef]
7. Wang, Y.; Zhang, R.; Chen, J.; Wu, H.; Lu, S.; Wang, K.; Li, H.; Harris, C.J.; Xi, K.; Kumar, R.V.; et al. Enhancing Catalytic Activity of Titanium Oxide in Lithium–Sulfur Batteries by Band Engineering. *Adv. Energy Mater.* **2019**, *9*, 1900953. [CrossRef]
8. Diamanti, M.V.; Ormellese, M.; Marin, E.; Lanzutti, A.; Mele, A.; Pedeferri, M.P. Anodic titanium oxide as immobilized photocatalyst in UV or visible light devices. *J. Hazard. Mater.* **2011**, *186*, 2103–2109. [CrossRef]
9. Kanna, M.; Wongnawa, S.; Buddee, S.; Dilokkhunakul, K.; Pinpithak, P. Amorphous titanium dioxide: A recyclable dye remover for water treatment. *J. Sol-Gel Sci. Technol.* **2010**, *53*, 162–170. [CrossRef]
10. Brunella, M.F.; Diamanti, M.V.; Pedeferri, M.P.; Di Fonzo, F.; Casari, C.S.; Li Bassi, A. Photocatalytic behavior of different titanium dioxide layers. *Thin Solid Films* **2007**, *515*, 6309–6313. [CrossRef]
11. Diamanti, M.V.; Ormellese, M.; Pedeferri, M.P. Application-wise nanostructuring of anodic films on titanium: A review. *J. Exp. Nanosci.* **2015**, *10*, 1285–1308. [CrossRef]
12. Diamanti, M.V.; Ormellese, M.; Pedeferri, M.P. Tuning of titanium oxide morphology at micro and nano scale by alternating current anodising. *J. Nano Res.* **2009**, *6*, 61–66. [CrossRef]
13. Diamanti, M.V.; Ormellese, M.; Pedeferri, M.P. Alternating current anodizing of titanium in halogen acids combined with anodic spark deposition: Morphological and structural variations. *Corros. Sci.* **2010**, *52*, 1824–1829. [CrossRef]
14. Diamanti, M.V.; Pedeferri, M.P. Effect of anodic oxidation parameters on the titanium oxides formation. *Corros. Sci.* **2007**, *49*, 939–948. [CrossRef]

15. Jáquez-Muñoz, J.M.; Gaona-Tiburcio, C.; Chacón-Nava, J.; Cabral-Miramontes, J.; Nieves-Mendoza, D.; Maldonado-Bandala, E.; Almeraya-Calderón, F. Electrochemical corrosion of titanium and titanium alloys anodized in H_2SO_4 and H_3PO_4 solutions. *Coatings* **2022**, *12*, 325. [CrossRef]
16. Kuromoto, N.K.; Simão, R.A.; Soares, G.A. Titanium oxide films produced on commercially pure titanium by anodic oxidation with different voltages. *Mater. Charact.* **2007**, *58*, 114–121. [CrossRef]
17. Maytorena-Sánchez, A.; Hernández-Torres, J.; Orozco-Cruz, R.; Zamora-Peredo, L.; López-Huerta, F.; Pacio-Castillo, M.; Serrano-de la Rosa, L.E.; Garcia-Gonzalez, L. Morphological and structural study of anodized titanium grade 2, using HCl in aqueous solution. *Mater. Res.* **2022**, *25*, e20210497. [CrossRef]
18. Ohtsu, N.; Komiya, S.; Kodama, K. Effect of electrolytes on anodic oxidation of titanium for fabricating titanium dioxide photocatalyst. *Thin Solid Films* **2013**, *534*, 70–75. [CrossRef]
19. Chelliah, N.M.; Saxena, A.; Sharma, K.; Singh, H.; Surappa, M.K. Surface characterization of nanoporous aluminium oxide films synthesized by single-step DC and AC anodization. *Surf. Interfaces* **2017**, *7*, 139–145. [CrossRef]
20. Kudelko, K.; Rozhdestvenskaya, L.; Ogenko, V.; Chmilenko, V. Formation and characterisation of porous anodized aluminum oxide, synthesized electrochemically in the presence of graphene oxide. *Appl. Nanosci.* **2022**, *12*, 1967–1976. [CrossRef]
21. Winiarski, J.; Tylus, W.; Pawlyta, M.; Szczygieł, B. Titanium anodization in deep eutectic solvents: The effect of anodizing time on the morphology and structure of anodic layers. *Appl. Surf. Sci.* **2022**, *577*, 151892. [CrossRef]
22. Vega, V.; Prida, V.M.; Hernandez-Vélez, M.; Mantova, E.; Aranda, P.; Ruiz-Hitzky, E.; Vazquez, M. Influence of anodic conditions on self-ordered growth of highly aligned titanium oxide nanopores. *Nanoscale Res. Lett.* **2007**, *2*, 355–363. [CrossRef]
23. Jain, S.; Williamson, R.S.; Roach, M.D. Surface characterization, shear strength, and bioactivity of anodized titanium prepared in mixed-acid electrolytes. *Surf. Coat. Tech.* **2017**, *325*, 594–603. [CrossRef]
24. Roach, M.D.; Williamson, R.S.; Blakely, I.P.; Didier, L.M. Tuning anatase and rutile phase ratios and nanoscale surface features by anodization processing onto titanium substrate surfaces. *Mater. Sci. Eng. C* **2016**, *58*, 213–223. [CrossRef] [PubMed]
25. Delplancke, J.-L.; Winand, R. Galvanostatic anodization of titanium—I. Structures and compositions of the anodic films. *Electrochim. Acta* **1988**, *33*, 1539–1549. [CrossRef]
26. Santos, E., Jr.; de Souza, G.B.; Serbena, F.C.; Santos, H.L.; de Lima, G.G.; Szesz, E.M.; Kuromoto, N.K. Effect of anodizing time on the mechanical properties of porous titania coatings formed by micro-arc oxidation. *Surf. Coat. Tech.* **2017**, *309*, 203–211. [CrossRef]
27. Galvis, O.A.; Quintero, D.; Castaño, J.G.; Liu, H.; Thompson, G.E.; Skeldon, P.; Echeverría, F. Formation of grooved and porous coatings on titanium by plasma electrolytic oxidation in H_2SO_4/H_3PO_4 electrolytes and effects of coating morphology on adhesive bonding. *Surf. Coat. Tech.* **2015**, *269*, 238–249. [CrossRef]
28. Liu, Z.; Thompson, G.E. Formation of porous anodic oxide film on titanium in phosphoric acid electrolyte. *J. Mater. Eng. Perform.* **2015**, *24*, 59–66. [CrossRef]
29. Root, N.V.; Kultin, Y.D.; Kustov, L.M.; Kudryavtsev, I.K.; Lebedeva, O.K. Effect of the conditions of anodizing on the morphology of nanotitania. *Russ. J. Phys. Chem.* **2017**, *91*, 213–216. [CrossRef]
30. Yamaguchi, K.; Konaka, Y.; Ohtsu, N. Effects of alcoholic solvents on the structure of anodized TiO_2 layer grown in nitrate electrolyte. *Surf. Coat. Tech.* **2020**, *387*, 125469. [CrossRef]
31. Ohtsu, N.; Ishikawa, D.; Komiya, S.; Sakamoto, K. Effect of phosphorous incorporation on crystallinity, morphology, and photocatalytic activity of anodic oxide layer on titanium. *Thin Solid Films* **2014**, *556*, 247–252. [CrossRef]
32. Zaniolo, K.M.; Biaggio, S.R.; Bocchi, N.; Rocha-Filho, R.C. Properties of colored oxide films formed electrochemically on titanium in green electrolytes under ultrasonic stirring. *J. Mater. Sci.* **2018**, *53*, 7294–7304. [CrossRef]
33. Regonini, D.; Bowen, C.R.; Jaroenworaluck, A.; Stevens, R. A review of growth mechanism, structure and crystallinity of anodized TiO_2 nanotubes. *Mater. Sci. Eng. R Rep.* **2013**, *74*, 377–406. [CrossRef]
34. Razzaboni, L.; Altomare, M.; Pedeferri, M.; Diamanti, M.V.; Schmuki, P. Hierarchical Anodic TiO_2 Nanostructures Formed in Ethylene Glycol/o-H_3PO_4 Electrolytes for Direct Photocatalysis. *ChemElectroChem* **2020**, *7*, 2859–2863. [CrossRef]
35. Raja, K.S.; Gandhi, T.; Misra, M. Effect of water content of ethylene glycol as electrolyte for synthesis of ordered titania nanotubes. *Electrochem. Commun.* **2007**, *9*, 1069–1076. [CrossRef]
36. Xie, Z.B.; Blackwood, D.J. Effects of anodization parameters on the formation of titania nanotubes in ethylene glycol. *Electrochim. Acta* **2010**, *56*, 905–912. [CrossRef]
37. Macak, J.M.; Schmuki, P. Anodic growth of self-organized anodic TiO_2 nanotubes in viscous electrolytes. *Electrochim. Acta* **2006**, *52*, 1258–1264. [CrossRef]
38. Guo, T.; Ivanovski, S.; Gulati, K. Fresh or aged: Short time anodization of titanium to understand the influence of electrolyte aging on titania nanopores. *J. Mater. Sci. Technol.* **2022**, *119*, 245–256. [CrossRef]
39. Lutterotti, L.; Matthies, S.; Wenk, H.R. MAUD: A friendly Java program for material analysis using diffraction. *IUCr Newsl. CPD* **1999**, *21*, 14–15.
40. Razaee, M.; Kohie, S.M.; Liu, K.H. The role of brookite in mechanical activation of anatase-to-rutile transformation of nanocrystalline TiO_2: An XRD and Raman spectroscopy investigation. *Cryst. Eng. Comm.* **2011**, *13*, 5055–5061. [CrossRef]
41. Spektor, K.; Tran, D.T.; Leinenweber, K.; Häussermann, U. Transformation of rutile to TiO_2-II in a high pressure hydrothermal environment. *J. Solid State Chem.* **2013**, *206*, 209–216. [CrossRef]

42. Makula, P.; Pacia, M.; Macyk, W. How to correctly determine the band gap energy of modified semiconductor photocatalysts based on UV–Vis spectra. *J. Fis. Chem. Lett.* **2018**, *9*, 6814–6817. [CrossRef] [PubMed]
43. Rudnev, V.S.; Medkov, M.A.; Lukiyanchuk, I.V.; Steblevskaya, N.I.; Kilin, K.N.; Belobeletskaya, M.V. Ta-containing coatings formed on titanium and stainless steel by plasma electrolytic oxidation and/or extraction pyrolysis. *Surf. Coat. Technol.* **2014**, *258*, 1232–1238. [CrossRef]
44. Guo, H.; An, M. Effect of surfactants on surface morphology of ceramic coatings fabricated on magnesium alloys by micro-arc oxidation. *Thin Solid Films* **2006**, *500*, 186–189. [CrossRef]
45. Zhu, X.; Liu, L.; Song, Y.; Jia, H.; Yu, H.; Xiao, X.; Yang, X. Oxygen bubble mould effect: Serrated nanopore formation and porous alumina growth. *Monatsh. Chem.* **2008**, *139*, 999–1003. [CrossRef]
46. Berger, S.; Kunze, J.; Schmuki, P.; Valota, A.T.; LeClere, D.J.; Skeldon, P.; Thompson, G.E. Influence of water content on the growth of anodic TiO_2 nanotubes in fluoride-containing ethylene glycol electrolytes. *J. Electrochem. Soc.* **2009**, *157*, C18. [CrossRef]